Landsat Instrument Suite (LandIS) sensor design for the Landsat 10 mission

Matthew Montanaro[a], Jeffrey Yee[b], Edmond Chung[b], Julie Montoya[b], Benjamin Turk[b], Eric Johnson[b], Andrew Pozo[b], Evan Haas[b], Steven Persh[b], Shawn Serbin[a], Thomas R. Holmes[a], Phillip W. Dabney[a], Bruce D. Cook[a], Christopher S.R. Neigh[a]

[a]*NASA Goddard Space Flight Center, Greenbelt, MD, USA*
[b]*Raytheon Company, El Segundo, CA, USA*

Abstract

Landsat 10 will be the upcoming mission in the 50+ year Landsat series of Earth observation platforms. The centerpiece of the observatory will be a super-spectral imager known as the Landsat Instrument Suite (LandIS). The sensor will feature 26 spectral channels from the visible through near-, short-wave, and thermal infrared wavelengths with spatial resolutions of 10, 20, and 60 meters on the ground, depending on the band. These enhancements over the legacy Landsat instruments will ensure data continuity with the existing archive and will expand upon the core Landsat capabilities to enable new applications in Earth science.

After a competitive procurement, NASA selected the design submitted by the Raytheon Company for the LandIS instrument. The innovative Raytheon instrument concept utilizes an advanced whiskbroom architecture to fulfill the strict radiometric, spatial, and geometric image quality requirements demanded by the Landsat 10 mission and fits within restrictive mass, volume, and power constraints. The instrument will continue the Landsat directive to image all daylit land and near-shore water areas, along with select nighttime imaging. On-board calibration source data will ensure high radiometric and geometric accuracy and stability consistent with previous missions to enable continuity in data products available to users. This paper discusses the driving requirements for LandIS and provides a description of the chosen design and operations concept of the instrument.

Keywords: Landsat 10, Landsat Instrument Suite (LandIS), Raytheon, Whisk-Broom, Instrument Design, Requirements

1. Introduction

Landsat 10, formerly Landsat Next [Cook et al. (2026)], will be the next observatory in the long-running series of joint NASA and USGS Landsat missions dating back to 1972 [Wulder et al. (2022)]. The Landsat program is highly regarded in the science community for its long-serving image archive, high radiometric and geometric accuracy, and publicly free data [Wulder et al. (2022, 2016); Crawford et al. (2023)]. With the exceptional accuracy and precision of its Earth science data, Landsat enables a wide range of critical applications that rely on identifying subtle shifts in surface reflectance or temperature [Hemati et al. (2021); Zhu (2017); Gök et al. (2024)]. In the 2010's, a comprehensive user needs and architecture study presented recommendations for the next mission after Landsat 9 [Wu et al. (2019)]. Requirements derived from these recommendations aimed to continue and enhance legacy Landsat science and applications but also add new capabilities mainly by incorporating new spectral bands and higher spatial resolutions. The Landsat Next mission was formulated around these requirements and intended to fly three observatories, each carrying an identical imaging sensor known as the Landsat Instrument Suite (LandIS). Currently, the triplet architecture has been re-planned to a single LandIS observatory known as Landsat 10.

The LandIS sensor will fulfill the imaging needs for Landsat 10 [NASA (2025)]. The instrument will be a "super-spectral" imager [NASA (2026)] covering 12 bands at visible/near-infrared (VNIR) wavelengths, 9 bands in the short-wave infrared (SWIR), and 5 bands in the thermal infrared (TIR) for a total of 26 spectral channels. These bands continue the legacy bands from Landsat 8 and 9; incorporate similar bands from the European Sentinel-2 Earth observation platform [Drusch et al. (2012)] to enhance harmonization of Landsat and Sentinel image products [Claverie et al. (2018); Ju et al. (2025)]; and expand spectral sampling to enable new science and applications such as emissivity estimation [Hulley et al. (2015)], atmospheric characterization [Vermote et al. (2018)], soil and crop residue characterization [Hively et al. (2021)], and enhanced water constituent retrieval [Ford and Vodacek (2020); Eon et al. (2026)], among others (Cook et al. 2026 provides a comprehensive overview of the science capabilities of the Landsat Next mission). In addition to enhanced spectral sampling, LandIS will have finer spatial resolutions over legacy Landsat instruments. When flying in the Landsat 10 orbit with a 653 km equatorial altitude, inclined at 98 degrees, LandIS image pixels will have ground sample distances (GSD) of 10, 20, and 60 meters. Importantly, LandIS image data must maintain continuity with the radiometric and geometric performance of the current instruments on Landsat 8 (L8) and Landsat 9 (L9). Lastly, due to the desire for lower launch costs, the instrument is constrained to smaller size, weight, and power (SWaP) requirements than recent Landsat instruments.

The set of instrument performance requirements, derived from mission requirements discussed in Cook et al 2026, are imposed on the calibrated image data from the instrument. Potential instrument vendors were tasked with designing a sensor that would acquire raw sample data of the Earth and produce radiometrically, spatially, and geometrically calibrated images that would meet all performance requirements while maintaining size, weight, and power constraints. The following sections discuss the key requirements that drive the design of the instrument and describe the resulting architecture chosen for the LandIS instrument.

2. Driving Requirements

Although LandIS will be an enhancement in terms of added spectral bands and finer spatial resolutions over previous Landsat instruments, the radiometric, spatial, and geometry requirements were developed with the core mantra of maintaining the equivalent on-orbit performance of L8 and L9. To facilitate this, the required performance for LandIS was derived by starting with the actual performance values for L8 (at 30 m VNIR/SWIR and 100 m TIR pixels) and scaling those values to the LandIS GSDs (10, 20, 60 m) and spectral bands. The intent was to make the LandIS image data equivalent to L8 image data if the LandIS data were aggregated to the L8 resolution and spectral bands. Note that not meeting the LandIS image requirements would mean that LandIS would not maintain performance continuity from the previous missions and would violate the core Landsat mission principle. A list of key radiometric and spatial requirements are listed in Table 1.

The demanding requirements for spectral coverage, pixel size, geometric and radiometric quality, along with tight SWaP constraints present a considerable challenge to build, test, and operate the LandIS instrument. The optimal design for one component might have a detrimental effect on other components. The final instrument design must balance all these competing requirements to ensure that all are met, even if not fully optimized. To this

Table 1: LandIS spectral band specifications and performance requirements. Note that the SNR requirements are specified at the reference radiance, L_{ref}. The highlighted bands indicate the approximate spectral bands on Landsat 8 and 9.

Band Number	Band Name	Band Center [nm]	Band Width [nm]	GSD [m]	Min. Edge Slope [1/m]	Signal-to-Noise Ratio (SNR)	L_{ref} [$W/m^2/sr/\mu m$]	L_{max} [$W/m^2/sr/\mu m$]
1	Violet	412	20	60	0.011	300	45	501
2	Coastal/Aerosol	443	20	20	0.033	330	129	551
3	Blue	490	65	10	0.066	293	128	578
4	Green	560	35	10	0.066	315	128	535
5	Yellow	600	30	20	0.033	300	118	489
6	Orange	620	20	20	0.033	200	21.5	397
7	Red 1	650	20	20	0.033	200	23	380
8	Red 2	665	30	10	0.066	260	108	443
9	Red Edge 1	705	15	20	0.033	253	74.5	417
10	Red Edge 2	740	15	20	0.033	220	68	378
11	NIR Broad	842	115	10	0.066	270	103	299
12	NIR 1	865	20	20	0.033	357	52.4	282
13	Water Vapor	945	20	60	0.011	227	9	239
14	Liquid Water	985	20	20	0.033	130	18	117
15	Snow/Ice 1	1035	20	20	0.033	130	16	177
16	Snow/Ice 2	1090	20	20	0.033	130	13	142
17	Cirrus	1375	30	60	0.011	200	6	107
18	SWIR 1	1610	90	10	0.060	87	4	72.4
19	SWIR 2a	2038	25	20	0.033	116	1.6	29.7
20	SWIR 2b	2108	40	20	0.033	116	1.5	24.6
21	SWIR 2c	2211	40	20	0.033	116	1.4	22.6
22	TIR 1	8300	250	60	0.01	260 (0.2 K)	9.38 (300 K)	24.7 (360 K)
23	TIR 2	8600	350	60	0.01	270 (0.2 K)	9.62 (300 K)	24.8 (360 K)
24	TIR 3	9100	350	60	0.01	283 (0.2 K)	9.87 (300 K)	23.9 (360 K)
25	TIR 4	11300	550	60	0.01	350 (0.2 K)	9.41 (300 K)	19.4 (360 K)
26	TIR 5	12000	550	60	0.01	370 (0.2 K)	8.96 (300 K)	17.9 (360 K)

end, the following requirement categories are key drivers for the instrument design:

Spectral Coverage The 26 spectral bands covering a wide range of wavelengths (VNIR/SWIR/TIR) necessitate detector materials and an optical system that can accommodate each wavelength regime. All spectral bands must be acquired within 15 seconds of each other.

Spatial Resolution The optical system, detector size, and sampling rate must be designed such that the processed (resampled) image pixels are at the required 10, 20, and 60 meter posts. Similarly, the edge response (*i.e.*, modulation transfer function, MTF) must accommodate these resolutions without blurring or aliasing [Burns et al. (2000); Fiete and Paul (2014)]. The required edge response for LandIS, measured as the minimum edge slope (the reciprocal distance between the 40% and 60% relative edge response), is equivalent to the L8/L9 edge performance. Note that the edge requirement for the SWIR1 band is slightly relaxed compared to the other 10 meter bands due to the difficulty of accommodating a 10 meter SWIR band with a broad-spectrum optical system.

Field of Regard (FOR) Radiometric uniformity of 0.5% variation must be maintained across the 14.4 degree swath (the same requirement as L8/L9 over its 15 degree swath) which influences the optical system and sampling architecture. Stray light must be less than 0.4% in the center of the field of view when surrounded by a source at L_{max} radiance (the same requirement as L8/L9).

Geometric Accuracy The pointing knowledge needed for tight band-to-band registration ($<$ 2 meters for the 10-meter bands) and image-to-image registration ($<$ 5 meters for the 10-meter bands) dictate highly precise mechanisms, sample timing, and mechanical and thermal stability. The geometric registration requirement was scaled to the finer LandIS GSD so that similar geometric performance of L8/L9 at 30 meter pixels is maintained for the LandIS 10 meter pixels (Note that the 20 and 60 meter bands are registered to the 10 meter bands).

Radiometric Response & Accuracy High signal-to-noise ratios (SNR) for narrower spectral bands and smaller GSDs demand low noise, highly efficient detectors along with a high throughput optical system and tight thermal control. SNR requirements were defined such that if LandIS pixels were aggregated to L8/L9 GSDs, they would provide nearly the same SNR. On-board calibration sources are needed to track radiometric stability ($<$ 0.5% VNIR/SWIR, $<$ 1% TIR) and maintain absolute accuracy ($<$ 5.5% for VNIR/SWIR, $<$ 2% for TIR, in radiance, worst-case) to enable measurement continuity from L8/L9 performance.

Mass/Volume/Power The physical size limitations (2.00 x 1.37 x 1.95 meters) defined for LandIS constrain the volume available for the optical system and on-board calibration sources. Mass restrictions ($<$ 550 kg) narrow options for materials and components. Power limits restrict resources for electronics and active thermal control.

Data Generation Rate The number of spectral bands and smaller GSDs result in much higher data rate than previous Landsat instruments (approximately 6x more than Landsat 9) and necessitate onboard data processing and lossy compression to fit prescribed downlink rates.

NASA solicited proposals from industry in the Spring 2023 for instrument designs that would accommodate these challenging requirements. After evaluating several competing instrument concepts, in June 2024 NASA selected the design proposed by the Raytheon Company for the LandIS instrument [NASA (2024)].

3. LandIS Design

LandIS will be a single whiskbroom-style imaging instrument to fulfill the needs of the Landsat 10 mission. Raytheon studied several potential instrument architectures including a whiskbroom, a pushbroom, and a step-stare design. The chosen scanning architecture offers advantages over other imaging styles by providing a cost-effective design that accommodates all LandIS radiometric, spatial, and geometric performance requirements while also fitting within the SWaP constraints.

Earlier Landsat instruments, including the Enhanced Thematic Mapper+ (ETM+) sensor on Landsat 7, have utilized the whiskbroom approach with a fast-scanning, single telescope optical design involving additional mechanisms to compensate for along-track orbital motion while imaging in the both the forward- and reverse-scan directions [USGS (2024); Markham et al. (2004)]. While all spectral bands (VNIR, SWIR, TIR) were imaged by a single instrument, the fast scan resulted in short integration times thereby limiting SNR and the complex mechanisms increased risk of on-orbit failure, particularly for Landsat 7 [Scaramuzza and Barsi (2005)]. The current Operational Land Imager (OLI) [Knight and Kvaran (2014)] and Thermal Infrared Sensor (TIRS) [Reuter et al. (2015)] instruments on Landsat 8 and 9 are of a pushbroom design that did not require any scan mechanisms and allowed for longer dwell times for increased SNR. However, the separate instruments for the VNIR/SWIR (OLI sensor) and for the TIR (TIRS sensor) spectral regions required a large spacecraft bus that could handle the footprints of the two instruments.

LandIS is effectively a hybrid of the previous instruments that incorporates the best aspects of the whisk- and pushbroom architectures but is contained within the limited size specification. The instrument will be a modern design that incorporates a single optical telescope with a simplified single-axis, slow scanning mechanism coupled with multiple staggered detector arrays utilizing digital time-delayed integration to maintain heritage SNR levels. This scanning arrangement produces a wide along-track footprint (reminiscent of a pushbroom) while imaging in the cross-track, forward scan direction before resetting for the next cross-track scan (see Section 4). The resulting dwell time is substantially increased over a traditional whiskbroom design but maintains the single telescope arrangement to accommodate imaging over all three spectral regions. The instrument also contains onboard radiometric calibration sources to track the short- and long-term accuracy and stability of the image data which is central to Landsat data continuity. Raytheon's design leverages scanning, detector, and calibration component heritage from current on-orbit imaging platforms such as the Visible Infrared Imaging Radiometer Suite (VIIRS) [Murphy et al. (2006)] and the WorldView Legion [Scott et al. (2020)] sensors and maximizes the use of other high technology readiness (TRL) components to reduce risk.

The LandIS instrument consists of several key components that work together to provide the necessary image data. Each major system is described below.

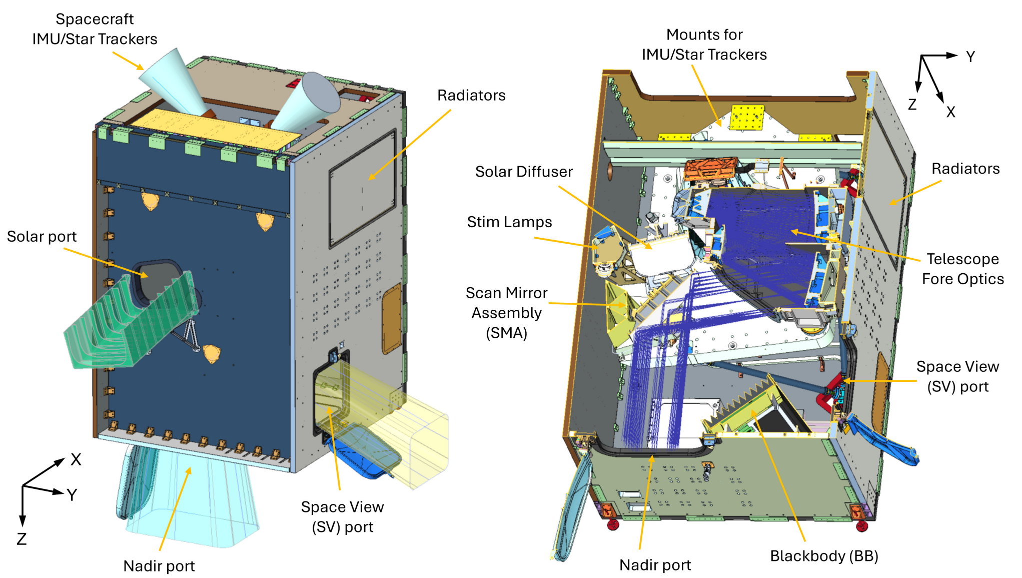

Figure 1: Diagram of the LandIS OMA outer structure (left) and interior cutaway (right).

Opto-Mechanical Assembly. The opto-mechanical assembly (OMA) structure contains all optical, mechanical, and electronic components and fits within the imposed size constraints. Inside the structure (see Figure 1), the optical/detector system is mounted to an optical bench assembly (the "strongback") that provides a stable platform for the optical train at a temperature of approximately 293 K. The radiator enclosure is the outer structure of the instrument that supports all thermal and electrical components and is mechanically tied to the strongback at three spacecraft interface fittings on the forward side of the structure, along with two additional monopod fixtures at the nadir corners for x-axis support. The instrument is intended to mount to the aft-facing surface (anti-ram) of the spacecraft bus to minimize orbital debris impacts. The nadir surface of the instrument has a clear view of Earth and contains the nadir viewing port with a deployable cover. Volume within the zenith-facing side of the instrument structure is allocated for spacecraft inertial measurement units (IMU)/star tracker components that mount directly to the strongback to reduce pointing knowledge uncertainty between the spacecraft motion sensing components and the instrument optical axis. Radiators mounted to the instrument structure provide heat rejection for the focal planes and electrical components.

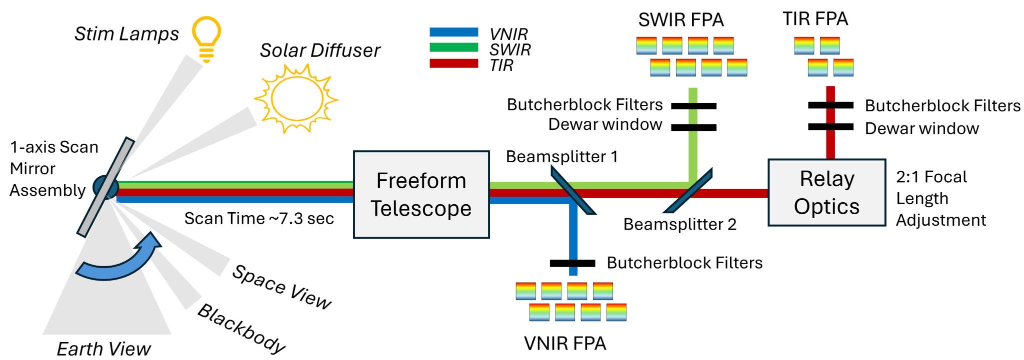

Figure 2: Illustration of the LandIS optical train. The SMA scans the Earth view, blackbody, and space view in one 7.3 second scan. Rays are focused by the telescope and split to the VNIR, SWIR, and TIR focal planes. The SMA periodically stares at the stim lamps or solar diffuser for image calibrations.

The optical and detector system consists of all components necessary to collect, focus, and detect incoming photons (see Figure 2). On one side of the strongback, the scan mirror assembly (SMA) contains a flat mirror mounted onto a single-axis, variable-speed mechanism that rotates in the cross-track direction. The SMA directs incoming photons from the nadir aperture, or from the calibration sources, into the telescope system. The fore optics are three powered, free-form mirrors with an effective focal length of 1.6 meters that focus and shape rays from the SMA to a fold mirror that directs rays to the underside of the strongback to the aft optics assembly (AOA). The AOA separates the incoming rays via Zinc Selenide (ZnSe) beamsplitters to three focal plane assemblies. The first beamsplitter reflects VNIR photons (short of approximately 920 nm) and directs them to the VNIR focal plane. SWIR and TIR photons are transmitted through this first beamsplitter and directed towards a second beamsplitter where SWIR photons are reflected towards a SWIR focal plane and TIR photons are transmitted. The TIR photons are then directed to a series of relay optics that halve the effective focal length (to 0.8 meters) before reaching the TIR focal plane.

Focal Plane Assemblies. The three focal plane assemblies (FPAs) cover the required 26 spectral band range for LandIS. Each contains multiple two-dimensional (2D) detector arrays with a 24-micron pixel pitch with digitization at the pixel cell. The arrays also utilize digital time delayed integration (TDI) with a selectable number of accumulation stages (up to 32 stages for the VNIR and SWIR arrays and up to 18 stages for the TIR arrays). The frame rates of the arrays are sufficient to sync with the scan mirror rate to ensure minimal scan motion blur. The VNIR focal plane is manufactured by Raytheon Vision Systems (RVS) and contains eight Silicon PIN (SiPIN) arrays with 672 by 448 active pixel elements that are staggered to provide a 4.5-degree along-track field of view (FOV). This arrangement, along with the scan mirror, effectively produces a push-broom scanning concept in the cross-track direction (see Figures 2 and 3). Butcher block spectral filters are mounted to the arrays to provide the necessary 12 VNIR spectral channels. Each filter covers multiple rows of pixel elements which may be used for TDI for that band. The detectors are passively cooled to approximately 255 K. The SWIR focal plane, also provided by RVS, similarly contains eight staggered arrays of the same dimensions but with Mercury Cadmium Telluride (HgCdTe) detector material with a 2.6 μm cutoff wavelength. The focal plane, with butcher block filters for the 9 SWIR channels, is contained within a vacuum dewar and cooled by a cryocooler to approximately 185 K. The TIR focal plane is manufactured by Teledyne Imaging Sensors (TIS) and contains four staggered HgCdTe detector arrays with 666 by 154 active pixel elements with a 24 micron pixel pitch and a 13.2 μm cutoff wavelength. The reduction of the focal length by the AOA TIR relay optics results in a doubling of the effective TIR pixel size relative to the VNIR and SWIR pixels so that only half the number of detector arrays are needed to cover the same 4.5 degree in-track FOV. Butcher block filters provide the 5 TIR spectral channels while the remaining area of the arrays are masked to provide a blind (dark) band to track the dark response of the arrays. The TIR focal plane is mounted inside its own dewar and cooled with a cryocooler to approximately 71 K. Both the SWIR and TIR dewars may be pumped to vacuum during ground testing to facilitate operation of the cryocoolers.

Onboard Calibration Sources. The instrument contains several calibration sources within its volume and within sight of the SMA for radiometric integrity and trending purposes (see Figures 1 and 2). Adjacent to the nadir aperture, a blackbody (BB) calibrator assembly is mounted to provide a warm TIR calibration source. The blackbody is based on the V-groove design from the VIIRS instrument and can be controlled anywhere between ambient temperature (low of 260 K) and 320 K, but will normally be controlled at 295 K. Next to the blackbody, on the +Y surface of the instrument, a space view (SV) aperture, with a deployable cover, offers a clear view of deep space to provide a dark and cold offset measurement. Opposite the nadir aperture toward the center of the instrument structure, two VNIR and SWIR calibration targets are mounted to the strongback. The first is a stim lamp assembly which contains a small parabolic mirror to collimate light from a number of incandescent lamps mounted inside an integrating sphere. When powered, the stim lamps illuminate the FOV of the VNIR and SWIR focal planes. The second source is a solar diffuser assembly which offers a full aperture illumination of a near-Lambertian diffuser plate. The diffuser is mounted at an angle between the line of sight of the SMA and a solar aperture port on the aft-facing (-X) panel of the instrument. A shutter mechanism opens to allow incoming solar irradiance to enter the instrument enclosure and reflect off the solar diffuser panel. This measurement requires the spacecraft to maneuver to allow the solar aperture to view the Sun.

Payload Electronics. The instrument electronics module, supplied by SouthWest Research Institute (SwRI), provides critical power, command, and data handling functions [Phelan et al. (2026)]. Mounted within the radiator enclosure, the payload electronics box contains several cards with specialized functions. The Low Voltage Power Supply distributes power from the spacecraft to the various LandIS components. The Single Board Computer (SBC) controls instrument functions and executes input commands and provides telemetry. The Analog I/O Boards and the Variable Heater Board provide active thermal management of the instrument components. The Motor Drive Board is responsible for mechanism control. Three Digital I/O Boards (DIB) provide input voltage and clocks to each of the three focal planes and buffer and process the raw pixel data from the detectors. The Compression Board takes formatted pixel samples from the DIBs, compresses and formats the image data, and transfers the compressed blocks across the spacecraft interface where they are stored by the mass storage device on the spacecraft, along with instrument telemetry from the SBC. In addition to the payload electronics components, a separate set of cryocooler electronics provides functions to operate the SWIR and TIR cryocoolers.

4. Operations Concept

As mentioned, the LandIS instrument operates as a slow-scan whiskbroom-style imager. As the spacecraft travels in orbit, the SMA rotates (scans) slowly in the cross-track direction while all three FPAs image the Earth during this forward scan. The imaging of the 164 km wide ground swath (+/- 7.2-degree nadir angle) is completed in approximately 5 seconds (see Figure 3). After imaging the Earth portion of the scan, the SMA scan rate then increases to quickly acquire image data of the BB and SV calibration sources before stopping and rapidly returning to its home position (without imaging during the return) to begin the next scan. This approximately 7.3 second scan period is repeated multiple times to cover the desired along-track interval on the Earth.

During a scan, the three focal plane arrays acquire pixel data at a frame rate that is aligned with the scan rate of the mirror to collect one integration per IFOV of the detector elements (approximately 3700 Hz for VNIR & SWIR, 1850 Hz for TIR). The scan rate and frame rate is adjustable to ensure an optimal sampling rate per latitude and to ensure a slight overlap in the along-track direction between consecutive scans. The native detector spacing on the ground in the Landsat 10 operational orbit is about 10 meters at nadir for the VNIR and SWIR detectors and 20 meters for the TIR detectors (due to the focal length adjustment by the TIR relay optics). The detector arrays utilize on-chip TDI to add multiple samples of the same location on the Earth to increase the SNR of the samples. As each frame (image line) is acquired from the FPAs, it is sent and stored as 15-bit integers in a buffer in the DIBs until the entire scan is stored as a 2D array per band.

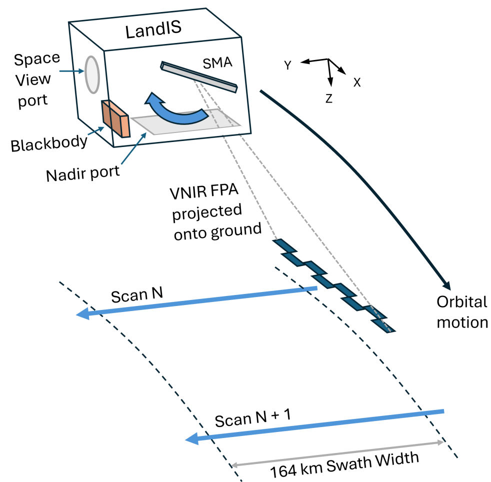

Figure 3: Illustration of the LandIS whiskbroom scanning concept. The SMA scans the 164 km Earth swath followed by a blackbody and deep space image acquisition before returning to the home position for the next scan.

As the SMA is reset to its home position for the next scan, the stored image data in the DIBs are processed and formatted. The leading and trailing image lines due to the staggered "saw tooth" arrangement of the detector arrays are trimmed off and the stored pixel data are aggregated (*i.e.*, binned or summed) to the required GSD for each band (*i.e.*, 1x1 binning for 10 meter; 2x2 binning for 20 meter; 6x6 binning for 60 meter; 3x3 binning for 60 meter TIR) and the binned values are truncated to 16 bits. To help increase the efficiency of the image compression, a non-uniformity correction (NUC) is applied to the aggregated pixels to reduce the spatial non-uniformity of the image data due to pixel-to-pixel gain differences. The image arrays are then formatted into image cubes of bands with the same GSD per detector array. The Earth pixel data cubes are sent to the compression board where they are compressed according to the CCSDS 123.0-B-2 standard. The compressed cubes are formatted with headers to identify them and sent over a gigabit ethernet (GbE) interface to the spacecraft for storage and transmission. Simultaneously, the SBC collects, formats, and transfers relevant instrument telemetry associated with the scan over the spacecraft interface. Pixel data from the BB and SV calibration sources (as well as the stim lamp and solar diffuser sources, when acquired) bypass the aggregation and compression steps and are transferred to the spacecraft in their native resolution.

The compressed Earth view (EV), uncompressed BB and SV, and instrument telemetry are eventually downlinked and processed on the ground to produce the Landsat 10 data products.

With 26 spectral bands plus the blind band at 10, 20, and 60 meter GSDs, 16-bit pixel data, and a 7.3 second scan, a large volume of data must be collected, formatted, compressed, and transferred in a short amount of time [Phelan et al. (2026)]. Data processing occurs in parallel as the next scan is acquiring image data. Two buffers in the DIBs work together so that one is processing the previous scan while the other is acquiring the current scan. Due to limited downlink capability, slightly lossy (*i.e.*, near-lossless) compression is configured to reduce data rates from LandIS to within acceptable margins without compromising scientific integrity of the pixel data [Eon et al. (2025)].

In concert with the nominal Earth scan, LandIS performs periodic special calibration acquisitions to provide data for trending and ground processing updates. The BB and SV are acquired every scan, as previously mentioned, and the data are used to remove the dark offset from the detector data and to track gain changes for the TIR focal plane. In addition to these nominal calibration acquisitions, the SMA is able to turn and stare at the stim lamp and solar diffuser assemblies when needed for VNIR and SWIR detector trending. Stim lamp data are expected to be acquired daily to track short term changes while a solar acquisition is planned weekly to allow for long term detector gain trending. Acquisitions of the onboard sources are also used to check detector operability for TDI selection. To track the degradation of the solar diffuser reflectance, monthly lunar acquisitions are planned in which the spacecraft is rotated to allow LandIS to view the Moon through the nadir aperture, similar to current Landsat reflective band calibration techniques [Angal et al. (2026)]. Lastly, LandIS is able to acquire image data at nighttime with all bands, or by deselecting unneeded bands, and is able to image off-nadir tracks (with a spacecraft roll maneuver) for targets of opportunity such as disaster response and monitoring.

5. Summary

The LandIS instrument will be the next generation Landsat imager. Earth image data produced by LandIS will add to the Landsat archive by continuing to support core Landsat applications but will add new capabilities with the increased spectral coverage and higher spatial resolutions. Demanding specifications for image quality and accuracy required by the Landsat program imposed challenges on instrument vendors to accommodate in their design concepts. The modern whiskbroom design by Raytheon for the LandIS instrument fulfills all Landsat image performance requirements within a cost-effective, modest size and weight footprint. The instrument will provide 26 VNIR, SWIR, TIR spectral channels with sharp edge responses for GSDs of 10, 20, and 60 meters. Onboard calibration sources along with a thermally stable optical and detector system enable accurate radiometric and geometric data to be produced that will be consistent with the Landsat archive. LandIS is expected to begin operations aboard the Landsat 10 mission in the early 2030s as the Landsat program approaches its 60th anniversary.

Funding

This work was funded under NASA contract numbers 80GSFC24CA038 and 80NSSC24K1205.

Acknowledgments

The authors thank personnel at Raytheon and their sub-contractors who are contributing to the design and development of the LandIS instrument for NASA. The authors also thank the NASA LandIS payload managers and systems engineers, past and present, for shepherding the procurement and development of LandIS for Landsat. Finally, the authors would like to acknowledge the NASA and USGS program managers, scientists, and support personnel who worked to define requirements for Landsat Next and helped guide the redesign of the project to what is now the Landsat 10 mission.

References

Angal, A., Miller, J., Thome, K., 2026. Radiometric calibration of OLI/OLI-2 reflective solar bands using the Moon. IEEE Transactions on Geoscience and Remote Sensing .

Burns, P.D., et al., 2000. Slanted-edge MTF for digital camera and scanner analysis, in: Is and Ts Pics Conference, Society for Imaging Science & Technology. pp. 135–138.

Claverie, M., Ju, J., Masek, J.G., Dungan, J.L., Vermote, E.F., Roger, J.C., Skakun, S.V., Justice, C., 2018. The Harmonized Landsat and Sentinel-2 surface reflectance data set. Remote sensing of environment 219, 145–161.

Cook, B.D., Roy, D.P., Masek, J.G., Wulder, M.A., Dabney, P.W., Neigh, C.S.R., Crawford, C.J., Holmes, T.R., Wu, Z., 2026. Landsat Next: Science requirements and mission architecture. Remote Sensing of Environment (in Revision) .

Crawford, C.J., Roy, D.P., Arab, S., Barnes, C., Vermote, E., Hulley, G., Gerace, A., Choate, M., Engebretson, C., Micijevic, E., et al., 2023. The 50-year Landsat collection 2 archive. Science of Remote Sensing 8, 100103.

Drusch, M., Del Bello, U., Carlier, S., Colin, O., Fernandez, V., Gascon, F., Hoersch, B., Isola, C., Laberinti, P., Martimort, P., Meygret, A., Spoto, F., Sy, O., Marchese, F., Bargellini, P., 2012. Sentinel-2: ESA's optical high-resolution mission for GMES operational services. Remote Sensing of Environment 120, 25–36.

Eon, R.S., De Groot, C., Pedelty, J.A., Gerace, A., Montanaro, M., Covington, R.K., DeLisa, A.S., Hsieh, W.T., Henegar-leon, J.M., Daniels, D.J., et al., 2025. Toward a near-lossless image compression strategy for the NASA/USGS Landsat Next mission. Remote Sensing of Environment 329, 114929.

Eon, R.S., Gartley, M.G., Holmes, T.R.H., Gerace, A., Montanaro, M., Serbin, S., Cook, B.D., 2026. Modeling polarimetric effects on aquatic remote sensing retrievals for Landsat 10. Optical Engineering 65, 073101.

Fiete, R.D., Paul, B.D., 2014. Modeling the optical transfer function in the imaging chain. Optical Engineering 53, 083103–083103.

Ford, R.T., Vodacek, A., 2020. Determining improvements in landsat spectral sampling for inland water quality monitoring. Science of Remote Sensing 1, 100005.

Gök, D.T., Scherler, D., Wulf, H., 2024. Land surface temperature trends derived from Landsat imagery in the swiss alps. The Cryosphere 18, 5259–5276.

Hemati, M., Hasanlou, M., Mahdianpari, M., Mohammadimanesh, F., 2021. A systematic review of Landsat data for change detection applications: 50 years of monitoring the Earth. Remote sensing 13, 2869.

Hively, W.D., Lamb, B.T., Daughtry, C.S.T., Serbin, G., Dennison, P., Kokaly, R.F., Wu, Z., Masek, J.G., 2021. Evaluation of SWIR crop residue bands for the Landsat Next mission. Remote Sensing 13.

Hulley, G.C., Hook, S.J., Abbott, E., Malakar, N., Islam, T., Abrams, M., 2015. The ASTER global emissivity dataset (ASTER GED): Mapping earth's emissivity at 100 meter spatial scale. Geophysical Research Letters 42, 7966–7976.

Ju, J., Zhou, Q., Freitag, B., Roy, D.P., Zhang, H.K., Sridhar, M., Mandel, J., Arab, S., Schmidt, G., Crawford, C.J., Gascon, F., Strobl, P.A., Masek, J.G., Neigh, C.S., 2025. The Harmonized Landsat and Sentinel-2 version 2.0 surface reflectance dataset. Remote Sensing of Environment 324, 114723.

Knight, E.J., Kvaran, G., 2014. Landsat-8 Operational Land Imager design, characterization and performance. Remote sensing 6, 10286–10305.

Markham, B.L., Storey, J.C., Williams, D.L., Irons, J.R., 2004. Landsat sensor performance: history and current status. IEEE transactions on geoscience and remote sensing 42, 2691–2694.

Murphy, R., Ardanuy, P., Deluccia, F.J., Clement, J., Schueler, C.F., 2006. The visible infrared imaging radiometer suite, in: Earth Science Satellite Remote Sensing: Vol. 1: Science and Instruments. Springer, pp. 199–223.

NASA, 2024. NASA selects Raytheon Company to build Landsat Next instruments. URL: `https://www.nasa.gov/news-release/nasa-selects-raytheon-company-to-build-landsat-next-instruments/`.

NASA, 2025. Landsat Instrument Suite (LandIS) Requirements Document (LaRD). Technical Report LNEXT-LANDIS-REQ-0007. NASA Goddard Space Flight Center.

NASA, 2026. Landsat 10. URL: `https://science.nasa.gov/mission/landsat-10/`.

Phelan, P., Koets, M., Hanley, J., Ford, J., Pozo, A., Bashir, A., Sarakasetrin, M., Keymeulen, D., Klimesh, M., Burchfiel, S., et al., 2026. Landsat Next Instrument Suite image processing & compression pipeline-from photons to bits and a story of data cubes, in: 2026 IEEE Aerospace Conference, IEEE. pp. 1–13.

Reuter, D.C., Richardson, C.M., Pellerano, F.A., Irons, J.R., Allen, R.G., Anderson, M., Jhabvala, M.D., Lunsford, A.W., Montanaro, M., Smith, R.L., et al., 2015. The Thermal Infrared Sensor (TIRS) on Landsat 8: Design overview and pre-launch characterization. Remote Sensing 7, 1135–1153.

Scaramuzza, P., Barsi, J., 2005. Landsat 7 scan line corrector-off gap-filled product development, in: Proceeding of pecora, pp. 23–27.

Scott, W.S., Anderson, N., Rogers, A.Q., 2020. Design drivers for a viable commercial remote sensing space architecture, in: 34th Annual Small Satellite Conference.

USGS, 2024. Landsat 7 (L7) data users handbook. URL: `https://www.usgs.gov/media/files/landsat-7-data-users-handbook`.

Vermote, E., Roger, J., Franch, B., Skakun, S., 2018. LaSRC (land surface reflectance code): Overview, application and validation using MODIS, VIIRS, Landsat and Sentinel 2 data's, in: IGARSS 2018 - 2018 IEEE International Geoscience and Remote Sensing Symposium, pp. 8173–8176.

Wu, Z., Snyder, G., Vadnais, C., Arora, R., Babcock, M., Stensaas, G., Doucette, P., Newman, T., 2019. User needs for future Landsat missions. Remote Sensing of Environment 231, 111214.

Wulder, M.A., Roy, D.P., Radeloff, V.C., Loveland, T.R., Anderson, M.C., Johnson, D.M., Healey, S., Zhu, Z., Scambos, T.A., Pahlevan, N., et al., 2022. Fifty years of Landsat science and impacts. Remote Sensing of Environment 280, 113195.

Wulder, M.A., White, J.C., Loveland, T.R., Woodcock, C.E., Belward, A.S., Cohen, W.B., Fosnight, E.A., Shaw, J., Masek, J.G., Roy, D.P., 2016. The global Landsat archive: Status, consolidation, and direction. Remote Sensing of Environment 185, 271–283.

Zhu, Z., 2017. Change detection using Landsat time series: A review of frequencies, preprocessing, algorithms, and applications. ISPRS Journal of Photogrammetry and Remote Sensing 130, 370–384.